Korean J. Chem. Eng., 38(3), 461-474 (2021)
DOI: 10.1007/s11814-020-0729-5

pISSN: 0256-1115
eISSN: 1975-7220

INVITED REVIEW PAPER

A short review on dissolved lithium polysulfide catholytes for advanced lithium-sulfur batteries

Rakesh Saroha*, Jou-Hyeon Ahn, and Jung Sang Cho*,†**

*Department of Engineering Chemistry, Chungbuk National University, Chungbuk 28644, Korea
**Department of Chemical Engineering, Gyeongsang National University, 501 Jinju-daero 52828, Korea
(*Received 7 October 2020 • Revised 9 December 2020 • Accepted 13 December 2020*)

Abstract−Lithium-sulfur battery (LSB) technology has drawn enormous attention during the last decade. Benefitting from the high theoretical specific discharge capacity (1,675 mAh g^{-1}) and energy density (2,600 Wh kg^{-1}), LSBs have proved to be a suitable candidate for electric vehicles and large-scale power grid electrical energy storage systems. However, the commercialization of LSB is hindered by various barriers, which include the high insulating nature of sulfur and its discharge products, severe polysulfide shuttling phenomenon, extreme volume expansion during charging/discharging, and poor stability of Li metal anodes. Additionally, LSB technology faces considerable battery design challenges, which allows high sulfur content and/or sulfur-loading while simultaneously maintaining a low electrolyte/sulfur ratio. Therefore, in this review, we highlight recent effective strategies that lead to more practical and commercial LSBs. We restrict ourselves to various cathode architectures designed specifically to absorb dissolved polysulfide catholyte. The integration of dissolved lithium polysulfide catholyte with specially designed cathode substrates efficiently allows ultra-high sulfur loading and/or sulfur-content with low electrolyte/sulfur ratio while still exhibiting reasonable electrochemical performance and cycling stability. The effect of concentration variation of dissolved lithium polysulfide catholyte on the cell performance is also discussed in detail. Therefore, the present review encapsulates feasible strategies with practical parameters to address the problems associated with LSBs.

Keywords: Lithium-sulfur Battery, Cathode, Lithium Polysulfide Catholyte, Electrochemical Performance, Practical Parameters

INTRODUCTION

The rapid consumption of fossil fuels and the associated environmental pollution has forced the search for other green energy technologies with higher efficiency and less hazardous nature that can be used for energy conversion and storage, such as supercapacitors and batteries [1-10]. Lithium-ion batteries (LIBs), based on intercalation electrochemistry, have already been established as forefront runners in today's battery market [11-16]. Launched back in the 1990s, LIBs provide a relatively high operating potential *vs.* Li/Li^+, high gravimetric/volumetric energy density, and stable cycling life [1,2,17-21]. However, LIBs are insufficient in energy and power density to power rapidly expanding sectors of portable electronics, electric vehicles (EVs), hybrid electric vehicles (HEVs), and grids [3,22-24]. The currently available commercial graphite/$LiCoO_2$ system has a much lower energy density (<250 W h kg^{-1}) than the required values in EVs and large grids [25]. Such hybrid systems require a much higher energy density at a lower cost compared with the presently available commercial LIBs to provide uninterrupted power back-up [26]. Therefore, exploring new technologies with matched energy and power density values is of utmost importance.

Among the currently existing alternatives to LIBs, lithium-sulfur batteries (LSBs) have attracted significant attention worldwide and emerged as a promising candidate for the next generation high energy density storage systems [27-33]. Unfortunately, the practical application of LSBs in the real world is currently hindered by a number of fundamental drawbacks. First, the low electrical conductivity of sulfur (5×10^{-30} S cm^{-1} at 25 °C) and Li_2S (10^{-13} S cm^{-1} at 25 °C) makes sulfur utilization difficult in the first step of the discharge curve, which continuously deteriorates during repeated cycling as sulfur is unable to accept electrons from the current collector [34-38]. In addition, the insulating Li_2S accumulates on the exterior of conductive matrix, leading to an abrupt drop in the cell voltage associated with high self-discharge or fast capacity fading [39-41]. Second, the intermediate long-chain lithium polysulfides (LiPSs, Li_2S_x; $4\leq x\leq 8$) generated during discharge process are highly soluble in the ether-based organic electrolytes, the most widely used electrolyte in LSBs [42-45]. These soluble and high-order polysulfides act as a double-edged sword in LSBs. They are beneficial in providing high sulfur utilization to some extent and increase reaction kinetics by providing good interaction with the conductive matrix [17]. However, the dissolution of LiPSs in the electrolyte introduces more disturbing challenges. Due to the concentration gradient, the dissolved LiPSs diffuse rapidly from the sulfur cathode and penetrate the separator to react with the Li metal anode and reduce to form short-chain LiPSs electrochemically, leading to the passivation of the anode with irreversible deposits on its surface [17,46-48]. Furthermore, a few parts of these short-chain LiPSs, travel back to the cathode under an induced electric field to be oxidized

†To whom correspondence should be addressed.
E-mail: jscho@cbnu.ac.kr

again to high-order LiPSs [17]. Thus, the generated high-order LiPSs again move towards the anode, reduce there to short-chain LiPSs and continue until the entire sulfur content is consumed. This vicious cycle of inter-conversion is well-known as the "shuttle effect" in LSBs [49-52]. This parasitic reaction results in a continued charging profile, low Coulombic efficiency, and fast capacity decay. The third is the significant volume expansion of sulfur over repeated cycling. During discharge, S_8 is converted to Li_2S through the intermediate LiPSs. The higher crystal density of sulfur (2.07 g/cm^3) compared to Li_2S (1.66 g/cm^3) leads to a significant volume expansion of ~80% [53-58]. The repeated expansion and contraction during continuous cycling results in pulverization/isolation of active materials, which results in poor reaction kinetics and fast capacity degradation. Finally, the low stability of Li metal anodes is another challenging issue in the development of stable LSBs. The reduction potential of Li metal is much lower (−3.045 V vs. Li^+/Li) than most of the solvents in the electrolytes, which leads to decomposition of electrolytes by forming a solid electrolyte interphase (SEI) [59]. However, pulverization of the active materials due to repeated cycling deteriorate the SEI layer, exposing the new Li metal surface, which leads to continuous consumption of the electrolyte, resulting in low Coulombic efficiencies of Cells [60,61].

To resolve the above-mentioned issues, a number of effective schemes have been adopted, which mainly includes the immobilization of LiPSs using physical (porous structured carbon hosts) and/or chemical (oxygenated functional groups, heteroatom doping, and polymer/metal oxide coating) means within a conductive framework such as metal compounds, carbon nanotubes, carbon nanofibers, and graphene/graphene oxides [49,62-71]. A schematic illustration of various carbon hosts for enhancing Li ion storage properties is shown in Fig. 1, which includes carbon hosts with different structure dimensions (0-D, 1-D, 2-D, 3-D), electrical conductivity (nitrogen-doped carbon, functional CNTs, etc.,) pore size (micro-, meso-, macro-) and various polar species (metal-oxides, -sulfides, -selenides) for efficient polysulfide anchoring. The development of specially designed carbon architecture is also reported [49,62-71]. For instance, Park et al. introduced a honeycomb-like N-doped carbon host, which is prepared using lignin followed by KOH activation [70]. Undoubtedly, the methods have tremendously enhanced the reaction kinetics and cycling performance of LSBs by improving the ionic and electronic conductivity of the sulfur-carbon framework and suppressing the lithium polysulfide diffusion by restricting them within the cathode domain. However, it is very difficult to completely immobilize the LiPSs due to the relatively weak interaction between the nonpolar carbon and polar LiPSs [72]. Moreover, the improvement in electrochemical performance in most of the previous works is generally achieved as a tradeoff for the impractical battery parameters needed for commercialization [73]. For instance, the typical sulfur loading in carbon-sulfur composites remains below 2.0 mg cm^{-2} with a sulfur content of less than approximately 70 wt% in the cathode [55,74-79]. Additionally, the amount of the electrolyte, i.e., electrolyte/sulfur (E/S) ratio, is also very high (more than 10 mL/g_{sulfur}) [80-83]. Low sulfur loading is generally associated with low areal capacity and poor energy density. Wang et al. reported that LSBs should deliver an areal capacity greater than 4 mAh cm^{-2} to be comparable with LIBs [84]. Furthermore, the sulfur content should not be lower than 70 wt% in the cathode to achieve a high volumetric energy density. So far, a sulfur content as high as 95 wt% in the electrode has been reported [85]. Similarly, a high electrolyte E/S ratio results in misleading extraordinary cell performance and compromises battery stability during the electrochemical process. For the unambiguous depiction of LSB electrochemical process, the amount of electrolyte inside the cell should not be higher than 4 mL/g_{sulfur} [17,86,87]. Overall, for LSBs to outperform commercial LIBs having an areal capacity ~4 mAh cm^{-2} with an average output voltage of ~3.6 V, the designed LSBs must have a sulfur content of at least 70 wt%, a sulfur loading of greater than 5 mg cm^{-2}, an areal capacity of over 6 mAh cm^{-2}, and an E/S ratio of not more than 4 mL/g_{sulfur} [87-89]. Despite many studies on LSBs, only a handful of articles have focused on addressing the critical parameters for practically viable LSBs.

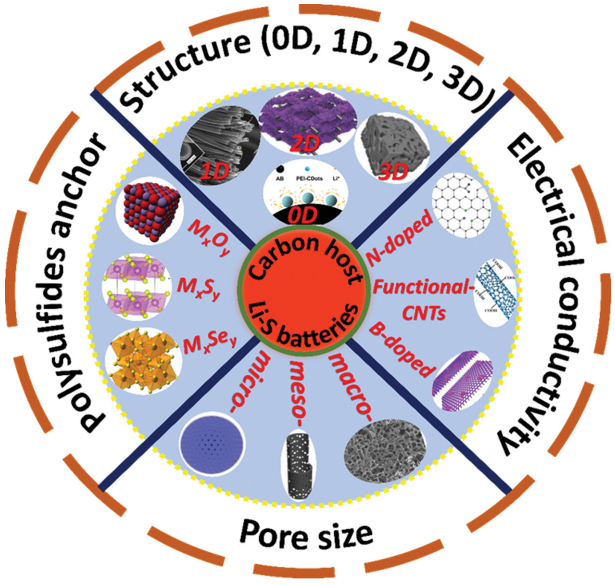

Fig. 1. Schematic illustration of various carbonaceous materials as cathode hosts for Li-S batteries classified according to structured type, electrical conductivity, pore size, and polysulfide anchor.

A novel approach of soluble polysulfide catholyte has recently gained worldwide attention instead of sulfur-carbon composites [90]. This facile strategy allows homogeneous dispersion of sulfur as active material in the conductive matrix, leading to higher utilization and enhanced battery performance [91]. Besides, incorporating a catholyte (i.e., a cathode present in liquid-phase) with different substrates such as a conductive carbon matrix effectively addresses issues such as ultra-high sulfur loading/content and low E/S ratio simultaneously while still exhibiting outstanding electrochemical performance and cycling stability [92]. Therefore, the purpose of this review is to provide a precise and exact overview of recent research achievements and effective strategies adopted for the development of advanced and practically feasible LSB technology entirely based on dissolved polysulfide catholyte and the respective Li-LiPS (Li-lithium dissolved polysulfide catholyte) cells.

We discuss the working of typical LSBs, followed by a brief

introduction and characteristics of lithium polysulfide catholyte. Afterward, relevant works on suitable cathode matrix/scaffolds are highlighted in line with dissolved polysulfide catholyte. Finally, we attempt to cover more crucial aspects of a viable lithium-sulfur batteries based on the dissolved polysulfide catholyte, i.e., catholyte concentration, and its effect on the electrochemical performance, sulfur content/loading based on the dissolved polysulfide catholyte, and finally, the E/S ratio. We believe that this review, which is explicitly based on Li-LiPS cells, will provide a fundamental direction or understanding for future research on developing feasible LSBs that involves catholyte.

WORKING PRINCIPLE OF LITHIUM-SULFUR BATTERIES (LSBs)

LSBs work on the reversible redox electrochemistry of elemental sulfur ($16Li^{+}+S_8+16e^{-}\leftrightarrow 8Li_2S$), thus yielding a high theoretical capacity of 1,675 mAh g^{-1} ($2e^{-}$ per sulfur atom) and high energy density of 2,600 W h kg^{-1} or 2,800 W h L^{-1} (considering the average cell voltage of 2.15 V), which can easily outperform commercialized LIBs (150-250 W h kg^{-1}) [53,93-98]. Moreover, LSBs differ from typical LIBs that work on the topotactic intercalation electrochemistry with reversible insertion and removal of Li-ions without

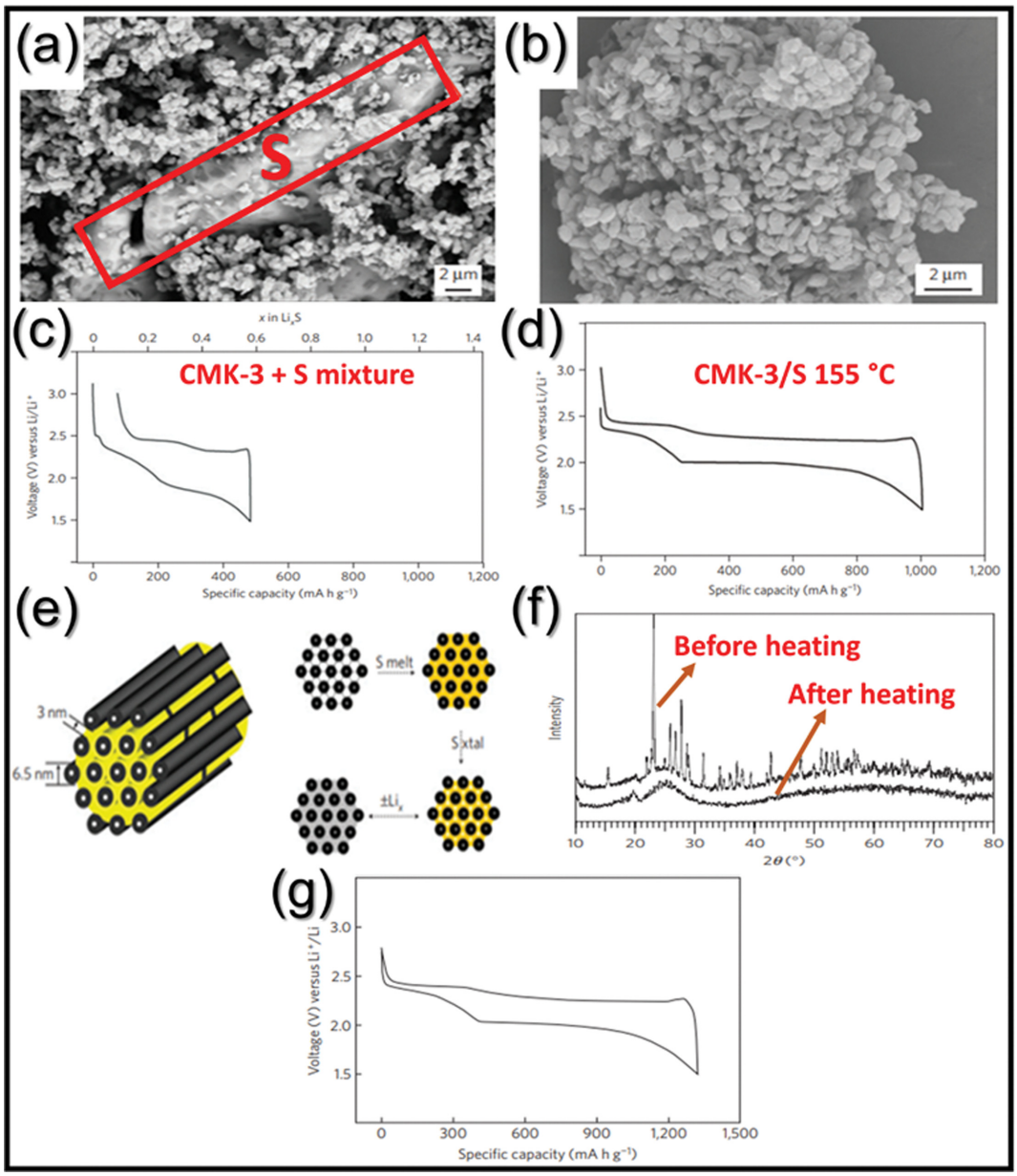

Fig. 2. (a) SEM image of CMK-3/Sulfur before heating, (b) CMK-3/Sulfur after heating at 155 °C, results in sulfur encapsulation, first charge-discharge profile of without heated CMK-3/Sulfur (c) and CMK-3/Sulfur heated at 155 °C (d) (current density=168 mA g^{-1}), (e) Schematic representation of sulfur encapsulation (yellow color) inside the interconnected mesopores structure of CMK-3, (f) XRD comparison of CMK-3/Sulfur before and after heating, and (g) charge-discharge profile of polyethylene glycol (PEG)-modified CMK-3/S-155 at 168 mAh g^{-1} (reproduced with permission from Ref. [103]).

changing the host structure [99]. Moreover, the natural abundance of sulfur (5th most common element on Earth) and inexpensiveness further proves its suitability for energy conversion and storage systems [99,100]. In the same manner as LIBs, the proof-of-concept of LSBs can also be traced back to the 1960s when lithium-sulfur cells were tested at high and consisted of sulfur as cathode and Li metal as the anode [101,102]. However, the early research on LSBs was phased out because of the poor cycling life of batteries that originated from the insulating nature of sulfur. It was only after the marvelous work conducted by Nazar et al. on LSBs in 2009 that this technology again came into the limelight of the world research community [103]. Nazar et al. reported a highly ordered nanostructured carbon-sulfur cathode, i.e., CMK-3/S, which demonstrated stable, high, reversible capacities (~1,320 mAh g^{-1}) with significantly improved cycling performance. The changes appearing in the CMK-3/S before and after heating at 155 °C can be clearly seen from the scanning electron microscopy (SEM) images shown in Fig. 2(a), (b). The complete disappearance of sulfur suggests that the elemental sulfur diffuses completely inside the mesopores of CMK-3 after heating. This difference in morphology is clearly reflected in the charge-discharge profile of the CMK-3/S sample obtained before and after heating (Fig. 2(c), (d)). The authors claim that the filling of mesoporous channels with sulfur provides inner pathways for the efficient diffusion of Li-ions, and mesoporous carbon effectively confines the polysulfide anions as shown in Fig. 2(e). The XRD results are also in good accordance with the above explanation (Fig. 2(f)). The authors further enhanced the electrochemical performance using surface functionalization by polyethylene glycol (PEG) coating over CMK-3 to trap the polysulfide species more effectively, which resulted in a very high discharge capacity of 1,320 mAh g^{-1} (Fig. 2(g)). This marvelous work opens up new frontiers for developing advanced strategies to further improve the electrochemical performance of LSBs.

After the work conducted by Nazar et al., LSBs have attracted tremendous attention and have undergone remarkable development. Fig. 3(a), (b) depicts a typical LSB working, which consists of a sulfur cathode, a soaked separator in an electrolyte, and a lithium metal anode. During lithiation (discharge), sulfur (cyclo-sulfur, S_8) reacts with lithium ions to form lithium sulfides through LiPSs [104]. The lithiation reaction takes place in four interrelated steps, which occur in different voltage ranges wherein sulfur is present in different phases (Fig. 3(b)) [104,105]. In the first step at 2.4 V, solid sulfur (S_8) reacts with lithium to form long-chain LiPSs (Li_2S_x; $6 \le x \le 8$) through a solid-liquid reaction mechanism. During the second step, i.e., in the range of 2.4-2.2 V, LiPSs formed in the first step are further reduced to short-chain polysulfides (Li_2S_x; $4 \le x \le 6$) via a liquid-liquid reaction process. These two steps generally account for the upper voltage plateau (or upper capacity region) with a total theoretical capacity contribution of 418 mAh g^{-1} (25% of theoretical value) [99,106]. The further reduction of lower order polysulfides (Li_2S_4) occurs at approximately 2.2 V to form Li_2S_x; x=2 or 1, as represented by a long plateau. A liquid-solid two-phase reaction process governs this step. In the last step, i.e., below 2.1 V, Li_2S_2 is reduced to Li_2S as an end product through a solid-solid reduction. The last two steps account for the remaining 75% of the theoretical capacity (1,257 mAh g^{-1}) [106]. This

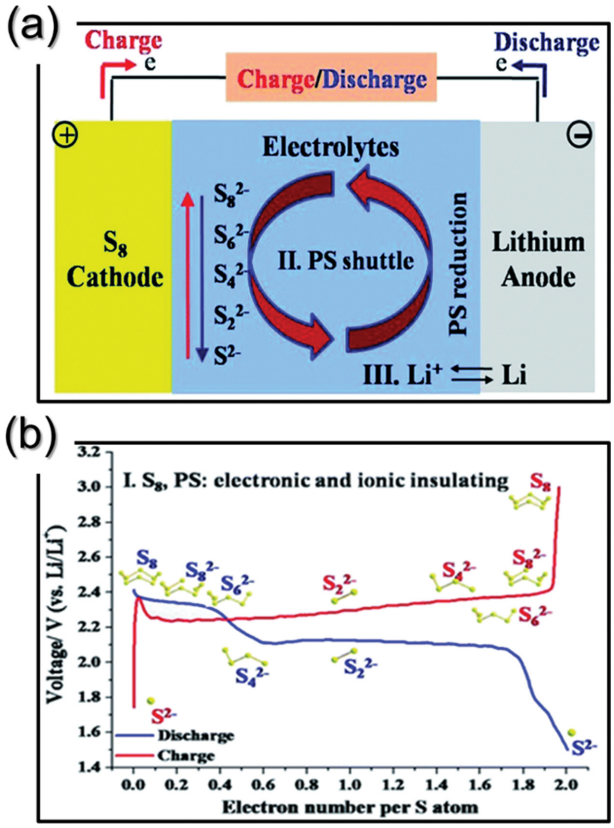

Fig. 3. (a) Working Mechanism of a Li-S battery involving formation of lithium polysulfides, (b) Charge/discharge profile showing contribution of different state of Sulfur during lithiation and delithiation (reproduced with permission from Ref. [105]).

multistep reduction process endows LSBs with an ultra-high specific discharge capacity of 1,675 mAh g^{-1} and an energy density of 2,600 W h kg^{-1} (with an average output voltage of around 2.15 V). In the following delithiation (charging) process, Li_2S is reversibly oxidized to elemental sulfur (S_8) through the formation of intermediate LiPSs (Li_2S_x; $4 \le x \le 8$). The following equations show the stepwise electrochemical reaction taking place in a typical LSB [107-111]:

$$S_8 + 2Li^+ + 2e^- \rightarrow Li_2S_8 \quad (1)$$

$$Li_2S_8 + 2/3Li^+ + 2/3\ e^- \rightarrow 4/3Li_2S_6 \quad (2)$$

$$Li_2S_6 + Li^+ + 2e^- \rightarrow 3/2Li_2S_4 \quad (3)$$

$$Li_2S_4 + 2/3Li^+ + 2/3e^- \rightarrow 4/3Li_2S_3 \quad (4)$$

$$Li_2S_3 + Li^+ + e^- \rightarrow 3/2Li_2S_2 \quad (5)$$

$$Li_2S_2 + 2Li^+ + 2e^- \rightarrow 2Li_2S \quad (6)$$

The intermediate long-chain LiPSs (Li_2S_x; $4 \le x \le 8$) generated during discharge are highly soluble in the ether-based organic electrolyte, the most widely used electrolyte in the case of LSBs. These soluble, high order polysulfides act as a double-edged sword in LSBs, which are beneficial in providing high sulfur utilization to some extent and increase reaction kinetics by providing good interac-

tion with the conductive matrix [17]. Nevertheless, their dissolution in the electrolyte brings more formidable challenges. In the next section, we will discuss polysulfide catholyte in more detail and its effect on the LSBs in terms of various parameters, such as concentration, sulfur content/loading, and electrolyte-sulfur ratio of polysulfide catholyte, which are beneficial for the assessment of LSBs with more practical parameters.

LITHIUM POLYSULFIDE CATHOLYTE

The use of dissolved polysulfide catholyte as an active cathode material in batteries was first reported by Rauh et al. in 1979 [112]. Among the most commonly used cathodes in LSBs under ambient conditions is elemental sulfur in the form of cyclo-S_8. As demonstrated in Fig. 3(a), (b) and Eqs. (1)-(6), during discharging, the cyclic-S_8 present in the crown-shaped structure tends to form polysulfide chains of different lengths (i.e., S_n^{2-}; n=1−8) in various voltage regions and the reverse occurs during charging. The di-radical sulfur atoms (i.e., S^-) present at the two ends of a nucleophilic polysulfide ion (S_n^{2-}) react with lithium to form different types of LiPSs with a general formula of Li_2S_n (n=1−8) [113]. The optimized molecular structure of different LiPS is shown in Fig. 4(a) [114,115]. Orthorhombic α-S_8 is the most stable allotrope of sulfur, which opens up during discharge and forms various LiPSs. Generally, S_8 exists in a puckered-type ring structure with D_{4d} crystal symmetry with S-S bond length around 2.06 Å [116]. Among these polysulfides, higher and middle-order LiPSs (i.e., Li_2S_8, Li_2S_6, and Li_2S_4) are highly soluble in the ether-based electrolytes solvents, which subsequently leads to the well-known "shuttle-effect" (Fig. 3(a)) [117]. Density functional calculations have revealed that soluble polysulfides exhibit C_2 crystal symmetry compared with other insoluble (or solid type) polysulfides that display C_{2v} symmetry [116]. The so-called polysulfide shuttling effect is responsible for the loss of active material and low sulfur utilization, leading to inferior electrochemical performance. Fig. 4(b) shows the various LiPSs dissolved in 1 M LiTFSI electrolyte, which displays different colors ranging from reddish-brown for the dissolved long-chain polysulfides to green-yellow for short-chain polysulfides [118]. It can be seen that higher-order polysulfides, i.e., Li_2S_8 and Li_2S_6, are completely soluble in organic electrolytes, whereas middle-order polysulfides, i.e., Li_2S_4 and Li_2S_2, are similar to a colloidal suspension and, therefore, partially soluble. On the other hand, lower-order Li_2S polysulfide is least soluble or insoluble in organic electrolytes. However, the solubility of middle-order polysulfides largely depends on their concentration and the type of solvent used. The typical solvent used for LSBs is 1,3-dioxolane/dimethyl ether (DOL/DME, 1 : 1, v/v) in which Li_2S_4 dissolves partially [118,119].

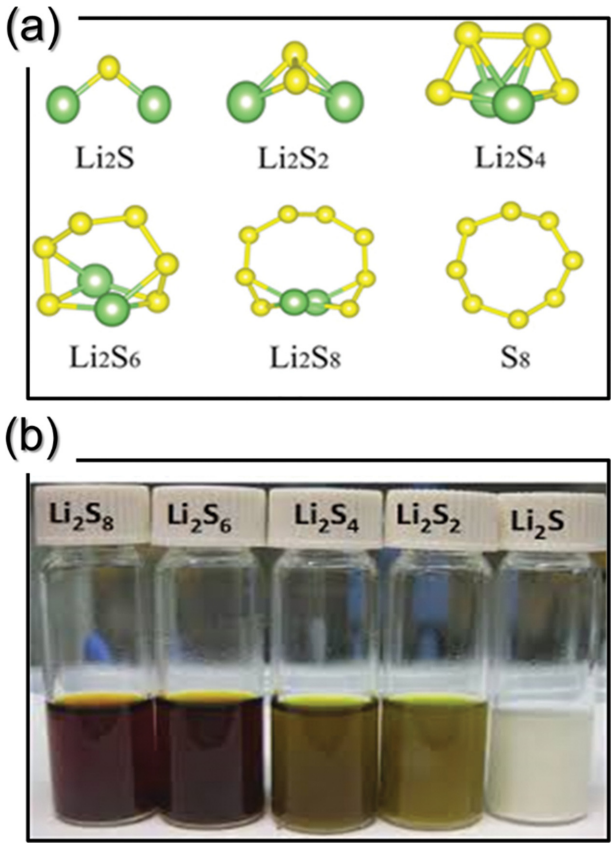

Fig. 4. (a) Molecular structure of various Lithium polysulfides (reproduced with permission from Ref. [114]), and (b) Visual demonstration of chemically synthesized different lithium polysulfides (i.e., Li_2S_n; n=1, 2, 4, 6, 8) in DOL/DME solvents with 0.2 M concentration calculated using elemental sulfur only (reproduced with permission from Ref. [118]).

Considering the soluble nature of higher order polysulfides, most research articles, therefore, have used Li_2S_8 or Li_2S_6 for the synthesis of lithium polysulfide catholyte. Although, among two polysulfides, Li_2S_6 is preferred for several reasons. First, the oxidation state of the sulfur atom in Li_2S_6 is −1/3, which lies between the lowest (−2) and highest (0) possible oxidation state for the sulfur atom. Therefore, the Li-dissolved polysulfide catholyte battery can be either discharged or charged first. Secondly, Li_2S_6 can bear the deviation of the lithium to sulfur ratio to maintain the equilibrium and solubility, which is evident from the following equation:

$$\text{Soluble } Li_2S + \text{insoluble S } (3\text{-}7) \rightarrow \text{Soluble } Li_2S_{6\pm2} \quad (7)$$

The above equation allows Li_2S_6 to exist in equilibrium with other higher-order soluble polysulfides [120]. Overall, the dissolved polysulfide catholyte solubility is the most important factor as it is directly associated with the uniform distribution of sulfur in the cathode region leading to high cathode capacity. Polysulfide catholyte concentration is another critical parameter that solely controls the capacity density of the cathode and, therefore, is on equal footing with the solubility parameter. Based on this discussion, we will discuss in detail the effect of concentration of dissolved polysulfide catholyte on the electrochemical performance of Li-LiPS cells. However, it is reasonable to discuss specially designed cathode substrates before catholyte parameters as the cathode architecture's physicochemical characteristics are the keys to improve Li-LiPS battery performance.

1. Specially Designed Cathode Substrates

In this section, we restrict ourselves to the cathode substrates that are designed specifically to absorb dissolved polysulfide catholyte. The cathode substrate or matrix acting as a sulfur host must possess few intrinsic characteristics such as sufficient porosity for

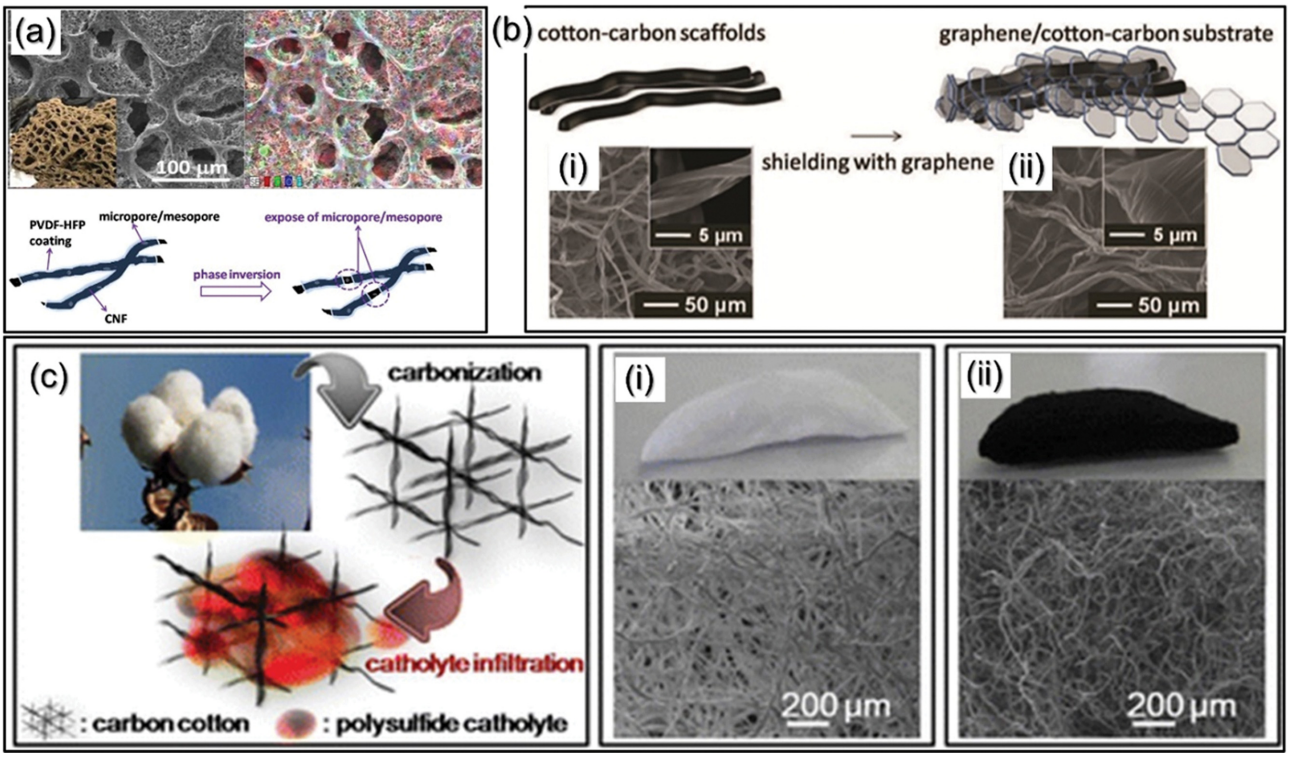

Fig. 5. Specially designed cathode substrates. (a) Microstructure analysis of an ant-nest-like (AN-like) cathode prepared using phase-inversion process and the corresponding elemental distribution (right panel), possible formation mechanism of nanopores during phase inversion (below panel) (reproduced with permission from Ref. [81]), (b) illustration of cotton-carbon/graphene synthesis and their respective microstructure, (i) cotton-carbon scaffolds and (ii) graphene/cotton-carbon matrix (reproduced with permission from Ref. [73]), and (c) Representation of the synthesis process for carbon-cotton cathodes, (i) Digital photographs of cotton (ii) and carbonized cotton (reproduced with permission from Ref. [121]).

efficient encapsulation of active material, and conductive pathways for Li-ion/electron transport. Likewise, the cathode skeleton must have sufficient chemisorption sites for trapping and reusing sulfur species during the charge-discharge process. Based on these parameters, Fig. 5(a)-(c) displays various cathode matrix structures specifically designed to withstand the high concentration and high sulfur content/loading of dissolved polysulfide catholyte. Fig. 5(a) represents the unique structural design of the cathode substrate using a facile synthesis approach, which is inspired by the ant-nest (inset image), and therefore, the authors named it as an "ant-nest-like" (AN-like) cathode [81]. The authors used poly(vinylidene fluoride-hexafluoropropylene) (PVDF-HFP) and carbon nanofibers (CNF) in a definite mass ratio to produce a free-standing thin film resembling an ant-nest-like structure. Based on the actual ant-nest structure, which possesses an open framework on the surface (pores with different diameters) and extends underneath, the interconnected structure was therefore believed to fulfill the requirement needed for a matrix to act as a sulfur host, i.e., storage (active material accommodation), blocking (LiPSs), and transport (Li-ion/electron). The phase-inversion technique is believed to entirely control the formation mechanism of the ant-nest-like structure as it allows the separation of polymer-rich (CNF/PVDF-HFP) and polymer-poor (NMP, *N*-methyl-2-pyrrolidone) phases through the exchange of solvent and non-solvent liquids (Fig. 5(a), lower panel). This controlled material synthesis of the cathode matrix resulted in the microporosity with fast diffusion of ions/electrons and more practical cell-fabrication parameters (discussed later in the following section).

A graphene/cotton-carbon structure and its microstructure analysis as a cathode substrate is represented in Fig. 5(b(i), (ii)) [73]. The graphene/cotton-carbon substrate provides enormous conductive pathways to outshine the insulating nature of elemental sulfur/Li_2S and active sites for efficient anchoring of dissolved polysulfides. Besides, the high conductive graphene was believed to induce a shielding effect on the carbon nanofiber (CNF) framework to prevent direct interaction with the dissolved polysulfide catholyte. However, this resulted in a decrease in the total surface area and pore volume of the synthesized cathode substrate compared with the pristine cotton-carbon substrate. Overall, the distinctive design results in improved electrochemical performances with more practical Li-LiPS features. Similar observations were recorded for the carbonized cotton substrate used as a cathode matrix for Li-LiPS cells (Fig. 5(c)) [121]. Although various carbon substrates are designed as a promising cathode host for Li-LiPSs electrochemistry, the non-polar nature of carbon hosts traps polysulfides that cannot be reutilized, which therefore inhibits the efficient conversion of polysulfides during cycles. To solve this problem, many unique structured polar cathodes are studied for Li-LiPSs cells, which include free-standing TiO_2 nanowire-embedded graphene hybrid membranes, TiS_2-polysulfide cathode encapsulated within a

carbon electrode shell, 3D structured rGO sponges, bacterial cellulose carbon nanofiber aerogel, Co-decorated N-doped carbon nanofiber membrane, 3D structured graphitic carbon foam-graphene@Mo_2C, and N, S-co-doped graphene sponges synthesized using hydrothermal reaction and freeze-drying [56,122-127]. Heng et al. reported a hybrid TiS_2-polysulfide cathode encapsulated within a carbon electrode shell, which showed a high areal capacity and energy density of 10 mAh cm^{-2} and 20 mWh cm^{-2}, respectively with a high sulfur content (65 wt%), high sulfur loading (12 mg cm^{-2}), and low E/S value (4.2 mL g^{-1}) [127]. Likewise, Zhou et al. developed a free-standing TiO_2 nanowire-embedded graphene (TiO_2 NW/G) membrane and utilized this polar cathode host for Li-LiPSs cell architecture. Li-LiPSs cell employing TiO_2 NW/G as a carbon host with a high sulfur content (62 wt%) and high sulfur loading (3.2 mg cm^{-2}) display stable cycling performances [128].

In general, cathode substrates with high porosity and pore volume are highly desirable for encapsulating an active material inside the designed substrate's micro and mesopores. However, such a high surface area also requires more electrolyte to fill the micropores for better reaction kinetics and stable cycling performance [129,130]. Therefore, there is always a tradeoff between the porosity and the amount of electrolyte consumed, which is also related to the concentration of polysulfides. Besides, high-concentration dissolved polysulfide catholyte (or high sulfur loading) is required for high energy density LSBs, which subsequently need more electrolyte volume to maintain a fixed E/S (electrolyte/sulfur) ratio.

2. Effect of Polysulfide Concentration on Cell Performance

It is necessary to do a comparative study of how the concentration of dissolved polysulfide catholyte could affect the electrochemical performance of Li-LiPS cells. As discussed above, lithium polysulfides are believed to form during the initial discharge according to Equations i-vi and diffuse through the separator to reach

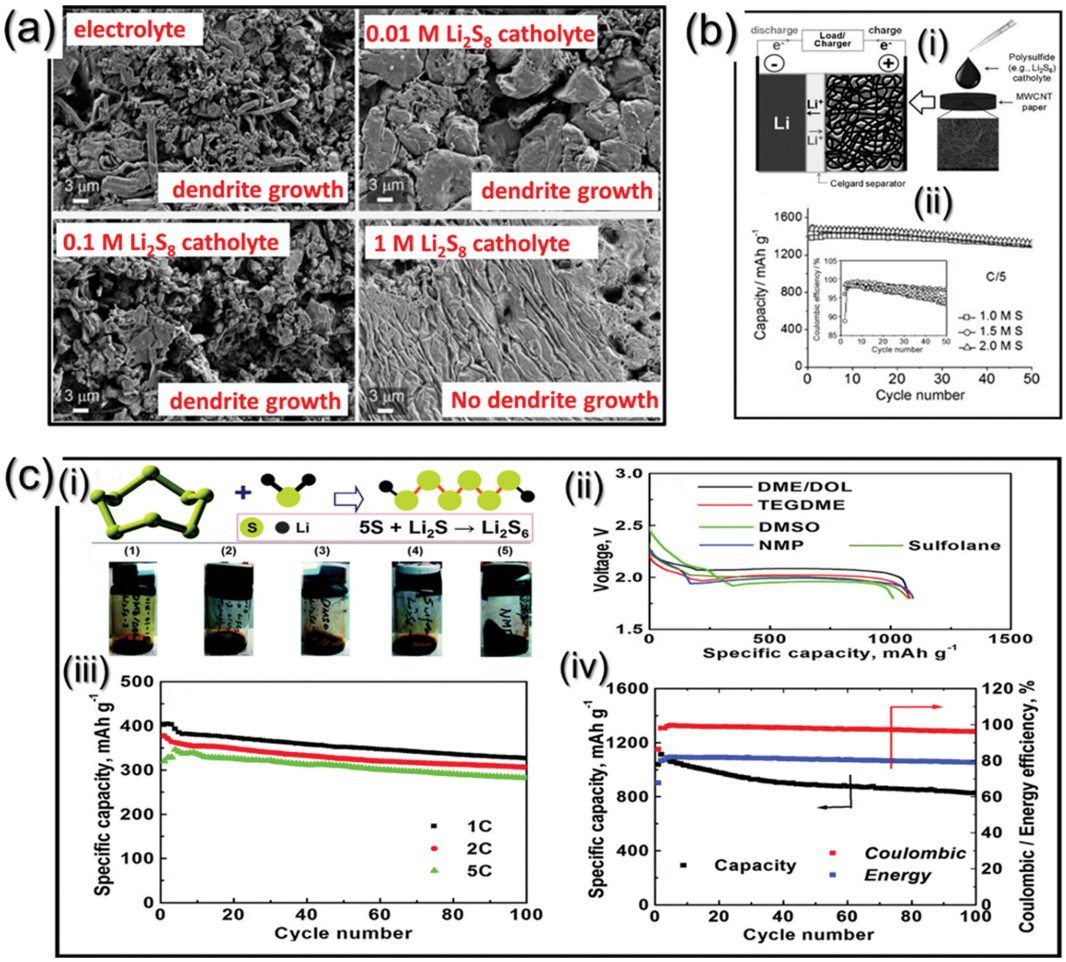

Fig. 6. (a) SEM images of Li anode obtained after 60 cycles of Li stripping and deposition with four different concentrations of polysulfide catholytes (reproduced with permission from Ref. [132]). (b) Schematic illustration of Li-polysulfide cell and free-standing MWCNT as electrode (i) and cycling performance of Li-dissolved polysulfide cells using different polysulfide concentration (1.0, 1.5, and 2.0 M of sulfur) at C/5 rate (ii) (reproduced with permission from Ref. [91]). (c) Li_2S_6 catholyte preparation in various solvents: (1) dimethoxy ethane /1,3-dioxolane (DME-DOL (1 : 1 v/v)), (2) tetraglyme (TEGDME), (3) dimethyl sulfoxide (DMSO), (4) tetra-methylene sulfone (sulfolane), and (5) *N*-methyl-2-pyrrolidone (NMP) (i), First discharge profiles of LSB at C/5 rate assembled using different catholytes with 4.0 M concentration of sulfur (ii), Graph between discharge capacity vs. cycle number at different C-rates with 4.0 M concentration of sulfur in the form of Li_2S_6 (iii), and Discharge capacity/ Coulombic efficiency vs. cycle number graph at C/5 rate for cells injected with 8.0 M concentration of sulfur (iv) (reproduced with permission from Ref. [119]).

the Li surface, resulting in the self-discharge phenomenon. Therefore, the polysulfide concentration in anodic region is of great importance as it considerably affects the Li-anode performance. Generally, polysulfide catholyte is prepared as a diluted solution with not more than 3.0 M of sulfur concentration [131]. However, there are reports in which polysulfide concentration used was as low as 0.01 M and as high as 8.0 M [119,132]. Talian et al. studied the effect of high-concentration polysulfides (1.0 M sulfur concentration in the form of Li_2S_8) on lithium stripping and deposition using electrochemical impedance spectroscopy (EIS) [132]. The group observed that the presence of high concentration polysulfides (1.0 M) effectively suppressed the lithium dendrite growth compared with the low concentration polysulfides (0.01 M and 0.1 M) (Fig. 6(a)). However, because of the volume limitation of cathode current collector to accommodate a liquid-phase polysulfide catholyte, it is very challenging to use high-molar polysulfide solutions.

Owing to the marvelous development of free-standing (3D-structures) cathodes with fine structure and high surface area, it is now possible to use and observe the effect of highly concentrated dissolved polysulfide catholyte on Li-LiPSs battery performance. Fu et al. reported a lithium/dissolved polysulfide cell based on self-weaving, free-standing multiwalled carbon nanotube (MWCNT) paper as a matrix for dissolved polysulfides with different sulfur concentration (1.0, 1.5, and 2.0 M) in the form of Li_2S_6 solution (Fig. 6(b)) [91]. The free-standing MWCNT electrode used was 40-50 μm thick, 1.2 cm in diameter, and 1.9-2.3 mg in mass (Fig. 6(b)(i)). The cyclic performance of the Li-LiPS cell at the C/5 rate with different concentration of the polysulfide catholyte is shown in Fig. 6(b)(ii). The authors attributed the Li-LiPS cell's excellent reversibility to the unique morphology of the highly integrated MWCNT electrode scaffold. Moreover, authors reported that to achieve good cyclability accompanied by high capacity, Li-LiPS cells employing MWCNT electrode and polysulfide catholyte must operate with ≤2 M of sulfur concentration at low or medium C-rates (<1.0 C). With higher polysulfide catholyte concentration (≥3 M) or high sulfur content (>60.0 wt%), the density difference between sulfur and its discharge product, i.e., Li_2S, leads to significant volume change during repeated charge-discharge and, hence, substandard discharge capacity or poor cycling. However, for ultra-high sulfur loading electrodes, polysulfide catholyte with extremely high concentration are desired.

The solubility of ultra-high concentration polysulfide strongly depends on the type of solvent used for catholyte preparation. In view of this, Manthiram et al. reported Li-LiPS battery performance using lithium polysulfide catholyte concentration as high as 8.0 M by employing multi-walled carbon nanotubes (MWCNTs) as free-standing electrodes [119]. The group studied the effect of different solvents on the voltage enhancement and cyclic performance of LSB. Fig. 6(c)(i) shows the Li_2S_6 polysulfide catholyte prepared using various solvents: (1) dimethoxyethane/1,3-dioxolane (DME-DOL), (2) tetraethylene glycol dimethyl ether (TEGDME), (3) dimethyl sulfoxide (DMSO), (4) sulfolane, and (5) *N*-methyl-2-pyrrolidone (NMP). The effect of various solvents on the discharge voltage, shown in Fig. 6(c)(ii), reveals that the DME-DOL and TEGDME solvents offer the highest discharge voltage. Similarly, the cyclability of cells injected with 4.0 M sulfur at different C-rates is shown in Fig. 6(c)(iii), which indicates no significant difference over prolonged cycling. Besides, Fig. 6(c)(iv) shows a graph between the discharge capacity and Coulombic and energy efficiencies when MWCNT current collectors were injected with 8.0 M concentration of sulfur in the form of Li_2S_6. The authors observed that the increase in capacity density from 2.85 mAh cm^{-2} (4.0 M concentration of sulfur) to 6.0 mAh cm^{-2} (8.0 M concentration of sulfur) had a minor impact on the cell performance, which indicates that high concentration polysulfides have huge potential for viable, high-energy-density LSB with practical parameters.

Although, an increase in the concentration of dissolved polysulfides beyond a certain limit results in high viscosities and, therefore, makes it difficult for polysulfides to disperse homogeneously in the cathode substrate [133-135]. Also, the higher concentration difference between bare electrolyte (usually 1.0 M) and a dissolved polysulfide catholyte leads to the higher dissolution of LiPSs in the cathode matrix according to Fick's law (Eq. (8)) and, therefore, a lower specific discharge capacity and decrease in capacity retention over prolonged cycling [136-138].

$$J = -D\frac{dC}{dx} \tag{8}$$

where J represents the diffusion flux ($cm^{-2}s^{-1}$), D is the diffusion coefficient (cm^2s^{-1}), and dC/dx is the concentration gradient. Apart from these reports, other works have employed different concentrations of dissolved LiPSs with a specially designed cathode matrix [56,92,124-126,133]. These studies indicate that the high-concentration polysulfide catholyte requires a suitable cathode substrate for a more uniform distribution of active material. Nevertheless, it is worth mentioning that the high concentration catholyte delivers ultra-high areal capacities. Based on this discussion, we attempt to cover the studies that have employed ultra-high sulfur content or loading based on dissolved polysulfide catholyte in the following section.

3. Effect of Sulfur Content/Loading on the Electrochemical Performance

There has been a significant improvement in the electrochemical performance of LSBs over the past decade, which exhibit experimental capacity (calculated on the mass of sulfur) approaching the theoretical capacity with stable cycling. However, these enhancements mainly originated due to the low sulfur content (<60 wt%) or active material loading (<7.0 mg cm^{-2}) in the cathode region, which subsequently led to low cathode resistance [73,139-141]. Therefore, it is highly desirable that the sulfur content in the cathode region should be sufficiently high to truly reflect the chemical and electrochemical state of LSBs. Based on the polysulfide catholyte as a sulfur source, a handful of studies have used high or ultra-high sulfur content to examine the electrochemical performance of Li-dissolved polysulfide cells. For instance, Yu et al. designed an ant-nest-like cathode as a conductive scaffold using a phase inversion process [81]. The obtained porous structure exhibited good rate capability at high sulfur content/loading, as shown in Fig. 7(a). Even at a high sulfur content of 75 wt% (11.5 mg cm^{-2}), Li-polysulfide cells showed slightly lower capacity compared with those at a sulfur content of 70 wt% (8.6 mg cm^{-2}). The high-rate perfor-

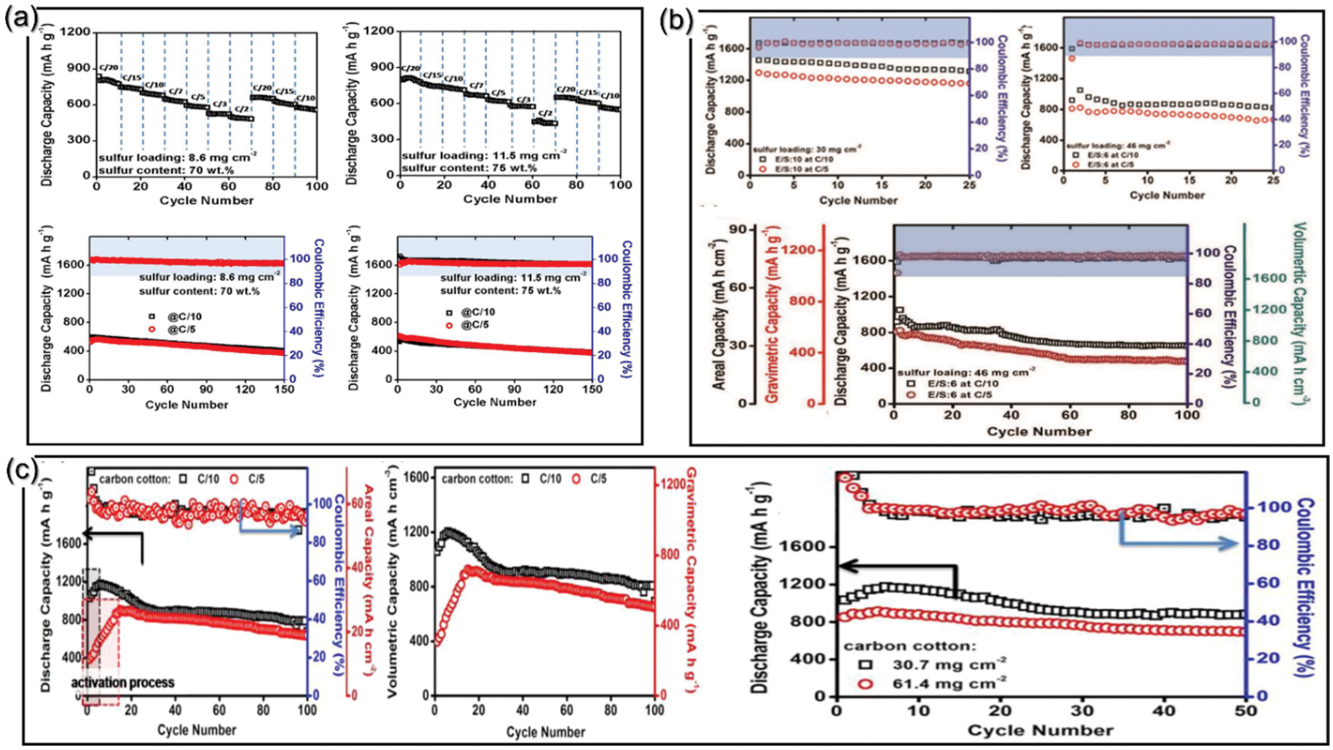

Fig. 7. (a) Rate capability of AN-like cathode with different sulfur loading/content of 8.6 mg cm^{-2}/70 wt% and 11.5 mg cm^{-2}/75 wt% (above panel), Cycling performance of AN-like cathode at 8.6 mg cm^{-2} and 11.5 mg cm^{-2} (below panel) (reproduced with permission from Ref. [81]). (b) Cyclability of graphene/cotton-carbon matrix at different sulfur loading and same sulfur content (60 wt%) with active material loading of 30 mg cm^{-2} and 46 mg cm^{-2} (above panel), long-term cycling performance at a high sulfur content/loading (70 wt%/46 mg cm^{-2}) shown at lower panel (reproduced with permission from Ref. [73]). (c) Dynamic cycling performance of carbon-cotton cathodes at C/10 and C/5 rates for 80 wt% sulfur content and 30.7 mg cm^{-2} sulfur loading (left), Volumetric capacity performance at identical rates (middle), and cycling performance for ultra-high sulfur content of 30.7 and 61.4 mg cm^{-2} (80 wt%) at C/10 rate (right) (reproduced with permission from Ref. [121]).

mance clearly envisaged a broad cycling performance, as displayed in Fig. 7(a) (lower panel). The authors attributed the excellent electrochemical performance of the Li-dissolved polysulfide cells to the unique structure of the cathode. The presence of macro-voids at the surface allowed high encapsulation of the active material, and fast ion/electron pathways resulted in superior cycling stability with low self-discharge. Likewise, Chung et al. reported a novel and facile approach to synthesize graphene/cotton-carbon cathode substrate that can withstand an ultra-high sulfur loading of 46 mg cm^{-2} (70 wt%) [73]. The respective electrochemical performance of the hybrid graphene/cotton-carbon matrix is shown in Fig. 7(b). The authors analyzed the electrochemical performance at different E/S ratio and observed that for an E/S ratio of 10 and sulfur loading of 30 mg cm^{-2}, the Li-LiPS cell delivered a discharge capacity of 1,450 and 1,300 mAh g^{-1} at C/10 and C/5 rates (left panel). When the E/S ratio was decreased to 6 and the loading was raised to 46 mg cm^{-2}, discharge capacity values were observed to be around 1,050 and 926 mAh g^{-1} at C/10 and C/5 rates (right panel). Besides, the Li-LiPS cell delivered enhanced battery performance (bottom panel) with practical parameters far above the standard values or the commercial graphite/$LiCoO_2$ arrangement. Thus, the designed cell exhibited an areal capacity of 35 mA h cm^{-2}, volumetric capacity of 881 mA h cm^{-3}, and energy density of 74 mW h cm^{-2} at C/5 rate with 46 mg cm^{-2} sulfur loading at a low E/S ratio of 5. The same group reported similar work with even more ultra-high sulfur content/loading of around 80 wt% (61.4 mg cm^{-2}) (Fig. 7(c)) [121]. These results clearly indicate that practically feasible LSB batteries can be designed by closely monitoring the hybrid cathode substrate with high conductivity and porosity, which allows fast redox reactions and ultra-high encapsulation of active material (sulfur in the form of dissolved polysulfide catholyte) with a low E/S ratio. In addition, a few more studies reported high sulfur content or active material loading with nearly practical features; however, these works are not as appealing as the above-mentioned studies [142,143]. Undoubtedly, high sulfur content and high loading are indispensable parameters for a practical LSB with high energy density; however, such a cell configuration cannot outperform a commercial LIB if it uses an excessive or low volume of electrolyte [144]. Therefore, we will next discuss the effect of E/S ratio on the electrochemical performance of Li-dissolved polysulfide catholyte.

4. Effect of Electrolyte/Sulfur Ratio

An electrolyte is generally considered an inactive component in a battery system that only acts as a medium for the smooth diffusion of ions during battery performance; therefore, it is not supposed to contribute to the electrochemical process. However, in

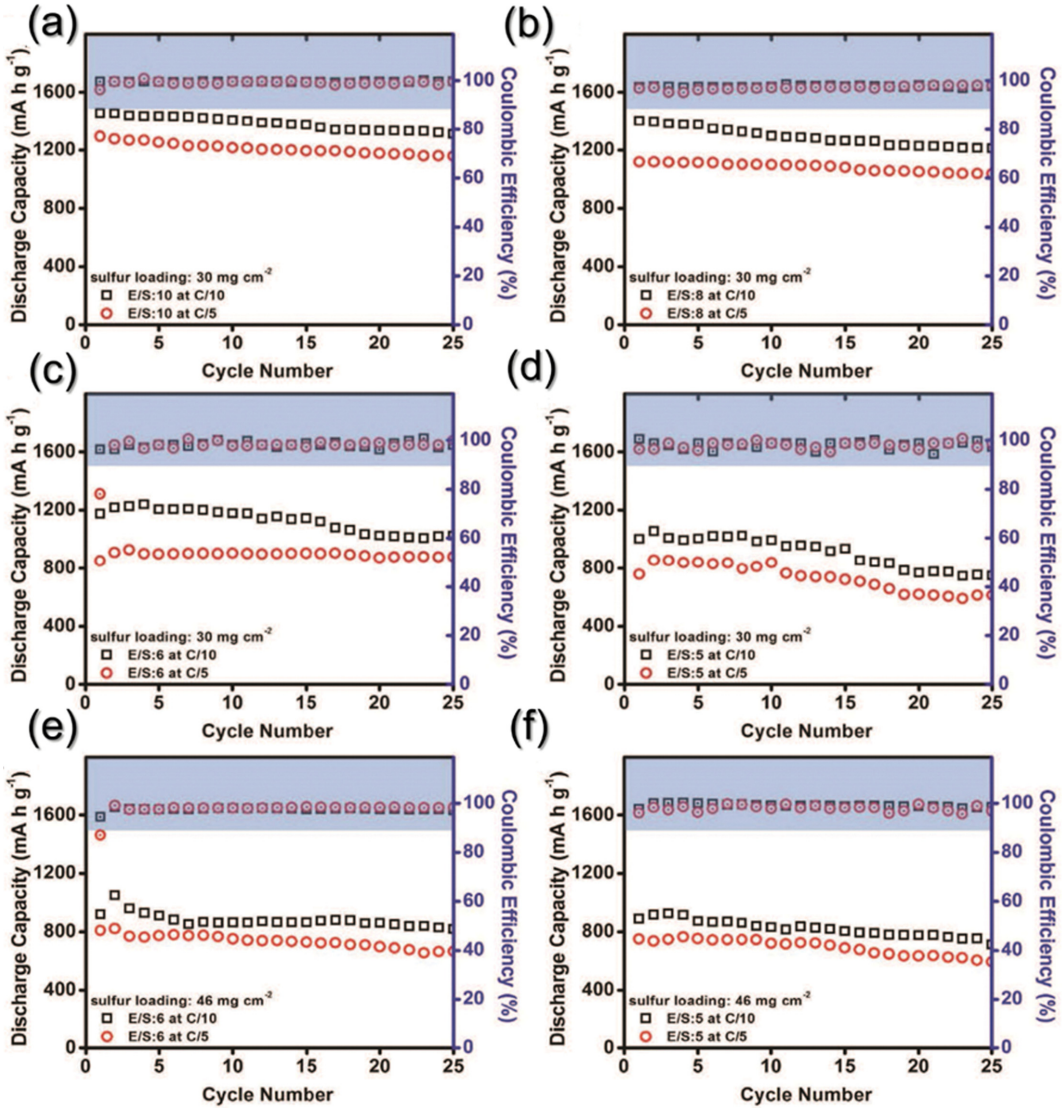

Fig. 8. Cycling performance of graphene/cotton-carbon cathode matrix with different E/S ratio at 30 (60 wt%) and 46 mg cm^{-2} (70 wt%) of sulfur loadings. (a) E/S=10, (b) E/S=8, (c) E/S=6, (d) E/S=5, (e) E/S=6, and (f) E/S=5 (reproduced with permission from Ref. [73]).

LSBs, the E/S ratio plays an essential role in sulfur utilization, reaction kinetics, and overall cell performance. Besides, this factor becomes more prominent if the active material is in dissolved polysulfide catholyte form. As the active polysulfides dissolve in the electrolyte itself to form a catholyte, the volume of the electrolyte in total increases significantly inside a Li-LiPS cell, which subsequently leads to higher inactive mass inside the cell. The ratio of electrolyte to sulfur commonly used in LSBs is more than 10 : 1 (i.e., 10 mL g^{-1}) in most of the studies [145]. However, for practical application, this ratio value should be as low as 4 mL g^{-1} for the high energy density of the cell [87]. Moreover, an ultra-low E/S value generally results in a high unutilized sulfur percentage because of inadequate electrode wetting, especially at high C-rates [143]. On the other hand, a high electrolyte volume indeed improves the reaction kinetics as it not only compensates for the electrolyte consumption, particularly for ultra-high sulfur electrodes, but also results in a decrease in the absolute energy density. Therefore, to obtain a high energy density with high sulfur loading, an optimum electrolyte volume is highly desirable. Manthiram et al. investigated the effect of different E/S ratios (10, 8, 6, and 5) on the electrochemical property of a graphene/cotton-carbon substrate employing a dissolved polysulfide catholyte as the active material (Fig. 8(a)-(f)) [73]. The sulfur content and sulfur loading were approximately 60 wt% and 30 mg cm^{-2}. For an E/S value of 10, the initial discharge capacity of about 1,450 and 1,300 mAh g^{-1} was obtained at C/10 and C/5 rates, respectively (Fig. 8(a)). With a decrease in the E/S ratio value to 6, the discharge capacity was found to decrease marginally, i.e., 1,240 mAh g^{-1}, at C/10 rate (Fig. 8(c)), which further reduces to 1,056 mAh g^{-1} at C/10 rate for an E/S ratio of 5 (Fig. 8(d)). The authors believe that the low nanoporosity could be the possible reason for the good electrochemical performance, especially at a low E/S ratio. Besides, even with an increase in sulfur loading from 30 to 46 mg cm^{-2} and sulfur content from 60 to 70 wt% for a low E/S value of 5, the Li-LiPS cells

Table 1. Comparison of electrochemical performance of various cathode hosts in terms of cathode host, sulfur loading, and E/S ratio

Cathode host	Sulfur/loading [wt%/mg cm^{-2}]	E/S [mL g^{-1}]	Initial capcity/ Rate [mAh g^{-1}/C]	Final capacity/Rate/ Cycle [mAh g^{-1}/C/–]	Final areal capacity/Rate/ Cycle [mAh cm^{-2}/C]	Ref.
Cobalt decorated N-doped C nanotubes	-/4.19	-	1166/0.2	938/0.2/300	- 5.46/0.2/100	[56]
Graphene/cotton C	70/46	5	765/0.2	750/0.2/25	25/0.1/100	[73]
Ant-nest-like C fiber/ PVDF-HFP	70/8.6	9	629/0.1	500/0/.1/150	- 7/0.2/-	[81]
3-D graphene sponge	-/2.2	-	1607/0.1	-/1.0/200	3.53/0.1/-	[124]
Cellulose carbon	80/2.74	-	1360/0.2	1033/0.2/200	-	[125]
Agaric-like Mo_2C/ graphene/ N-doped C foam	70/3.5	10	862/1.0	597/600/1.0	- 10.2/0.1/100	[126]
TiO_2 nanowire embeded graphene	62/3.2	20.8	1270/0.2	1053/0.2/200	-	[145]
Core-shell structured C	70/17.3	8	639/0.1	447/0.1/100	7.7/0.1/100 9.3/0.1/100	[146]
3-D structured C paper	80/17	3.9	593/0.1	545/0.1/100	9.3/0.1/100	[147]
rGO/CNTs aerogel embedding FeP nanocubes	60/2.4	-	950/1.0	800/1.0/500	8.5/0.2/50	[150]
Vertically alligned carbon nanotubes	-/2.3	-	775/0.02	550/0.02/50	4/0.1/50	[151]

delivered discharge capacity of approximately 926 and 765 mAh g^{-1} at C/10 and C/5 rates, respectively (Fig. 8(f)). These results clearly suggest that the combined strategy of synthesizing advanced cathode substrates employing a dissolved polysulfide catholyte could result in more viable Li-LiPS cells with ultra-high sulfur loading, high sulfur content, and low E/S ratio. In a similar work, Xiao et al. discussed the influence of the sulfur/electrolyte (S/E) ratio on the electrochemical performance of LSB [146]. However, they used a sulfur composite for their study instead of a dissolved polysulfide catholyte. Overall, the E/S ratio is a crucial parameter for determining the stable electrochemical performance with better protection of Lithium anode, especially at a low E/S ratio. Table 1 compares the overall electrochemical performance of various cathode hosts for LSBs reported in the literature in terms of various key parameters. The high sulfur content, high sulfur loading, and low E/S ratio are crucial parameters to determine the actual efficiency of the Li-S battery system. In general, low sulfur loading is associated with the poor energy density and low areal capacity of LSBs. Additionally, LSBs recommend providing an areal capacity of at least 4 mAh cm^{-2} for comparison with the current commercial $LiCoO_2$-graphite system [147,148]. As presented in the Table 1, most of the works show areal capacity value higher than 4.0 mAh cm^{-2}. Among all, Chung et al. reported a graphene/cotton-carbon cathode with ultra-high loading of 46 mg cm^{-2} with an overwhelming areal capacity value of 25 mAh cm^{-2}, which is 6.25-times higher than that of LIBs. Additionally, the cathode showed ultra-high energy density values of around 74 mA h cm^{-2}, which is almost 7 - higher than the LIBs (10.0 mW h cm^{-2}). The results clearly suggest that the rational design of the Li-S nanostructured hosts not only envisages the feasibility of viable metal-sulfur batteries but also outperforms the presently available commercial LIBs architecture.

FUTURE CHALLENGES AND RESEARCH DIRECTIONS

The feasibility of LSBs based on a dissolved polysulfide catholyte as an active material (Li-LiPSs) for commercial applications such as large-scale grids and EVs/HEVs can be realized only by optimizing battery characteristics in terms of high sulfur loading, high sulfur content, and low E/S ratio. Above all, an advanced cathode substrate with a highly porous structure that can accommodate a high amount of an active material, tolerate large volume variations, and provide sufficient conductive channels for the smooth diffusion of lithium-ions during the charge-discharge process is highly indispensable. Therefore, we believe that this review paper provides preliminary directions for developing viable Li-dissolved polysulfide catholyte batteries that can offer atypical electrochemical performance and can compete with presently available LIB technology.

One of the biggest challenges LSBs based on a dissolved polysulfide catholyte face is the development of a flexible power supply. As the majority of the active material is present in the form of a catholyte, which is dissolved in the electrolyte itself, the total volume of the liquid component inside the Li-LiPS cells is very high, which causes safety issues for the development of future portable/ wearable electronic devices. Therefore, more efforts are needed in the development of standard designs with clearly tested benchmarks for porosity/surface area, flexibility, active material loading

and E/S ratio. Such flexible high energy density Li-LiPS cells could be a potential alternative for future electronic and unmanned devices that require high power and volumetric energy density to operate.

Another challenge that requires cutting edge research is the smooth functioning of Li-LiPS cells at high temperature (≤50 °C). At high temperature, a fraction of electrolyte, which is present in high volume inside the cell, could evaporate and increase the cell's total vapor pressure, which poses a threat to the cell. By using suitable electrolytes with optimized solvents, more realistic and safer Li-LiPS cells can be imagined. Therefore, to expand the commercial application of Li-LiPS cells, the critical issues mentioned above must be addressed satisfactorily.

ACKNOWLEDGEMENTS

This work was supported by the National Research Foundation of Korea (NRF) grant funded by the Korea government (MSIP) (NRF-2018R1A4A1024691, NRF-2017M1A2A2087577, NRF-2018R1D1A3B07042514). This research was also supported by Chungbuk National University (2019).

REFERENCES

1. P. H. Wadekar, A. Ghosh, R. V. Khose, D. A. Pethsangave, S. Mitra and S. Some, *Electrochim. Acta*, **344**, 136147 (2020).
2. B. Li, Y. Pan, B. Luo, J. Zao, Y. Xiao, S. Lei and B. Cheng, *Electrochim. Acta*, **344**, 135811 (2020).
3. S. Jiang, M. Chen, X. Wang, P. Zeng, Y. Li, H. Liu, X. Li, C. Huang, H. Shu, Z. Luo and C. Wu, *Electrochim. Acta*, **313**, 151 (2019).
4. R. Saroha, A. Gupta and A. K. Panwar, *J. Alloys Compd.*, **696**, 580 (2017).
5. R. Saroha, A. K. Panwar, Y. Sharma, P. K. Tyagi and S. Ghosh, *Appl. Surf. Sci.*, **394**, 25 (2017).
6. K.-J. Lee, T.-K. Kim, S. Koomson and C.-G. Lee, *Korean J. Chem. Eng.*, **35**, 2010 (2018).
7. L. Fan, P. Sun, L. Yang, Z. Xu and J. Han, *Korean J. Chem. Eng.*, **37**, 166 (2020).
8. S. Ghosh, W. D. Yong, E. M. Jin, S. R. Polaki, S. M. Jeong and H. Jun, *Korean J. Chem. Eng.*, **36**, 312 (2019).
9. S. Ghosh, S. M. Jeong and S. R. Polaki, *Korean J. Chem. Eng.*, **35**, 1389 (2018).
10. Y.-K. Lee, S. Chung, S. Y. Hwang, S. Lee, K. S. Eom, S. B. Hong, G. G. Park, B.-J. Kim, J.-J. Lee and H.-I. Joh, *Korean J. Chem. Eng.*, **36**, 1543 (2019).
11. B. Zheng, L. Yu, N. Li and J. Xi, *Electrochim. Acta*, **345**, 136186 (2020).
12. Z. Jian, H. Li, R. Cao, H. Zhou, H. Xu, G. Zhao, Y. Xing and S. Zhang, *Electrochim. Acta*, **319**, 359 (2019).
13. R. Saroha and A. K. Panwar, *J. Phys. D Appl. Phys.*, **50**, 255501 (2017).
14. H. Park, D. H. Yeom, J. Kim and J. K. Lee, *Korean J. Chem. Eng.*, **32**, 178 (2015).
15. N. Venugopal, W.-S. Kim and T. Yu, *Korean J. Chem. Eng.*, **33**, 1500 (2016).
16. H. S. Kang, P. Santhoshkumar, J. W. Park, G. S. Sim, M. Nanthagopal and C. W. Lee, *Korean J. Chem. Eng.*, **37**, 1331 (2020).
17. Z.-L. Xu, J.-K. Kim and K. Kang, *Nano Today*, **19**, 84 (2018).
18. R. Saroha, A. K. Panwar and Y. Sharma, *Ceram. Int.*, **43**, 5734 (2017).
19. K.-M. Kang, H.-W. Kim and H.-Y. Kwak, *Korean J. Chem. Eng.*, **33**, 688 (2016).
20. D.-L. Vu and J.-w. Lee, *Korean J. Chem. Eng.*, **33**, 514 (2016).
21. Q. N. Tran, I. T. Kim, J. Hur, J. H. Kim, H. W. Choi and S. J. Park, *Korean J. Chem. Eng.*, **37**, 898 (2020).
22. L. Wang, Z.-Y. Wang, J.-F. Wu, G.-R. Li, S. Liu and X.-P. Gao, *Nano Energy*, **77**, 105173, (2020).
23. Y. Zhou, H. Shu, Y. Zhou, T. Sun, M. Han, Y. Chen, M. Chen, Z. Chen, X. Yang and X. Wang, *J. Power Sources*, **453**, 227896 (2020).
24. H. S. Ko, H. W. Park, G. J. Kim and J. D. Lee, *Korean J. Chem. Eng.*, **36**, 620 (2019).
25. Z.-Y. Wang, D.-D. Han, S. Liu, G.-R. Li, T.-Y. Yan and X.-P. Gao, *Electrochim. Acta*, **337**, 135772 (2020).
26. W. Li, Z. Chen, D. Wang, Z. Gong, C. Mao, J. Liu, H. Peng, Z. Zhang and G. Li, *J. Power Sources*, **435**, 226778 (2019).
27. L. Shi, F. Zeng, X. Cheng, K. H. Lam, W. Wang, A. Wang, Z. Jin, F. Wu and Y. Yang, *Chem. Eng. J.*, **334**, 305 (2018).
28. J. Wang, L. Gao, C. Gu, J. Wang and J. Huang, *J. Electroanal. Chem.*, **877**, 114565 (2020).
29. H. Wang, B. Zhang, X. Zeng, L. Yan, J. Zheng, M. Ling, Y. Hou, Y. Lu and C. Liang, *J. Power Sources*, **473**, 228588 (2020).
30. D. Di Lecce, V. Marangon, W. Du, D. J. L. Brett, P. R. Shearing and J. Hassoun, *J. Power Sources*, **472**, 228424 (2020).
31. J. Li, L. Zhang, F. Qin, B. Hong, Q. Xiang, K. Zhang, J. Fang and Y. Lai, *J. Power Sources*, **442**, 227232 (2019).
32. G. Tonin, G. B. M. Vaughan, R. Bouchet, F. Alloin, M. Di Michiel and C. Barchasz, *J. Power Sources*, **468**, 228287 (2020).
33. S. Chen, Y. Ming, B. Tan and S. Chen, *Electrochim. Acta*, **329**, 135128 (2020).
34. Y. Zhong, X. Xu, Y. Liu, W. Wang and Z. Shao, *Polyhedron*, **155**, 464 (2018).
35. T. Wu, G. Sun, W. Lu, L. Zhao, A. Mauger, C. M. Julien, L. Sun, H. Xie and J. Liu, *Electrochim. Acta*, **353**, 136529 (2020).
36. C. Huang, T. Sun, H. Shu, M. Chen, Q. Liang, Y. Zhou, P. Gao, S. Xu, X. Yang, M. Wu, J. Jian and X. Wang, *Electrochim. Acta*, **334**, 135658 (2020).
37. C. Huang, Y. Zhou, H. Shu, M. Chen, Q. Liang, S. Jiang, X. Li, T. Sun, M. Han, Y. Zhou, J. Jian and X. Wang, *Electrochim. Acta*, **329**, 135135 (2020).
38. J. Wang, Y. Liu, M. Cheng, H. Zhao, J. Wang, Z. Zhao, X. Duan, C. Wang and J. Wang, *Electrochim. Acta*, **318**, 161 (2019).
39. Z. Zhao, G. Li, Z. Wang, M. Feng, M. Sun, X. Xue, R. Liu, H. Jia, Z. Wang, W. Zhang, H. Li and Z. Chen, *J. Power Sources*, **434**, 226729 (2019).
40. F. Zhou, Z. Qiao, Y. Zhang, W. Xu, H. Zheng, Q. Xie, Q. Luo, L. Wang, B. Qu and D.-L. Peng, *Electrochim. Acta*, **349**, 136378 (2020).
41. E. V. Kuzmina, E. V. Karaseva, D. V. Kolosnitsyn, L. V. Sheina, N. V. Shakirova and V. S. Kolosnitsyn, *J. Power Sources*, **400**, 511 (2018).
42. A. Raulo, S. Bandyopadhyay, S. Ahamad, A. Gupta, R. Srivastava, P. Formanek and B. Nandan, *J. Power Sources*, **431**, 250 (2019).
43. J.-W. Guo and M.-S. Wu, *Electrochim. Acta*, **327**, 135028 (2019).
44. S. Liu, Y. Li, C. Zhang, X. Chen, Z. Wang, F. Cui, X. Yang and W. Yue, *Electrochim. Acta*, **332**, 135458 (2020).

45. S. Li, X. Chen, F. Hu, R. Zeng, Y. Huang, L. Yuan and J. Xie, *Electrochim. Acta*, **304**, 11 (2019).
46. Z. W. Lu, Y. H. Wang, Z. Dai, X. P. Li, C. Y. Zhang, G. Z. Sun, C. S. Gong, X. J. Pan, W. Lan, J. Y. Zhou and E. Q. Xie, *Electrochim. Acta*, **325**, 134920 (2019).
47. M.-S. Kim, M. S. Kim, V. Do, Y. Xia, W. Kim and W. I. Cho, *J. Power Sources*, **422**, 104 (2019).
48. J. Long, H. Zhang, J. Ren, J. Li, M. Zhu, T. Han, B. Sun, S. Zhu, H. Zhang and J. Liu, *Electrochim. Acta*, **356**, 136853 (2020).
49. W. Li, J. Hicks-Garner, J. Wang, J. Liu, A. F. Gross, E. Sherman, J. Graetz, J. J. Vajo and P. Liu, *Chem. Mater.*, **26**, 3403 (2014).
50. K. Kim, P. J. H. Kim, J. P. Youngblood and V. G. Pol, *ChemSusChem*, **11**, 2375 (2018).
51. A. A. Razzaq, Y. Yao, R. Shah, P. Qi, L. Miao, M. Chen, X. Zhao, Y. Peng and Z. Deng, *Energy Storage Mater.*, **16**, 194 (2019).
52. S. Dai, Y. Feng, P. Wang, H. Wang, H. Liang, R. Wang, V. Linkov and S. Ji, *Electrochim. Acta*, **321**, 134678 (2019).
53. F. Jin, S. Xiao, L. Lu and Y. Wang, *Nano Lett.*, **16**, 440 (2015).
54. Y. Li, T. Jiang, H. Yang, D. Lei, X. Deng, C. Hao, F. Zhang and J. Guo, *Electrochim. Acta*, **330**, 135311 (2020).
55. Y. Pei, Y. Wang, Y. Darraf, A.-Y. Chang, H. Zhao, X. Liu, J. Liu, Y. Lvov and S. Wang, *J. Power Sources,* **450,** 227698 (2020).
56. S. Yao, R. Guo, F. Xie, Z. Wu, K. Gao, C. Zhang, X. Shen, T. Li and S. Qin, *Electrochim. Acta*, **337**, 135765 (2020).
57. Z. Wu, L. Yuan, Q. Han, Y. Lan, Y. Zhou, X. Jiang, X. Ouyang, J. Zhu, X. Wang and Y. Fu, *J. Power Sources*, **450**, 227658 (2020).
58. J. Kim, D. Byun, H.-S. Kim, W. Choi and S.-O. Kim, *J. Power Sources*, **427**, 165 (2019).
59. B. Liu, R. Fang, D. Xie, W. Zhang, H. Huang, Y. Xia, X. Wang, X. Xia and J. Tu, *Energy Environ. Mater.*, **1**, 196 (2018).
60. D. Lin, Y. Liu and Y. Cui, *Nat. Nanotechnol.*, **12**, 194 (2017).
61. Y. Liu, D. Lin, Z. Liang, J. Zhao, K. Yan and Y. Cui, *Nat. Commun.*, **7**, 10992 (2016).
62. S. Xin, L. Gu, N.-H. Zhao, Y.-X. Yin, L.-J. Zhou, Y.-G. Guo and L.-J. Wan, *J. Am. Chem. Soc.*, **134**, 18510 (2012).
63. Z. Peng, W. Fang, H. Zhao, J. Fang, H. Cheng, T. N. L. Doan, J. Xu and P. Chen, *J. Power Sources*, **282**, 70 (2015).
64. Y. Xu, Y. Wen, Y. Zhu, K. Gaskell, K. A. Cychosz, B. Eichhorn, K. Xu and C. Wang, *Adv. Funct. Mater.*, **25**, 4312 (2015).
65. A. Rosenman, E. Markevich, G. Salitra, Y. Talyosef, F. Chesneau and D. Aurbach, *J. Electrochem. Soc.*, **163**, A1829 (2016).
66. J.-Q. Huang, Q. Zhang and F. Wei, *Energy Storage Mater.*, **1**, 127 (2015).
67. Z. Zhang, Y. Lai, Z. Zhang, K. Zhang and J. Li, *Electrochim. Acta*, **129**, 55 (2014).
68. Z. Hao, R. Zeng, L. Yuan, Q. Bing, J. Liu, J. Xiang and Y. Huang, *Nano Energy*, **40**, 360 (2017).
69. T. Chen, L. Ma, B. Cheng, R. Chen, Y. Hu, G. Zhu, Y. Wang, J. Liang, Z. Tie and J. Liu, *Nano Energy*, **38**, 239 (2017).
70. J. S. Yeon, S. H. Park, J. Suk, H. Lee and H. S. Park, *Chem. Eng. J.*, **382**, 122946 (2020).
71. J. S. Yeon, S. Yun, J. M. Park and H. S. Park, *ACS Nano*, **13**, 5163 (2019).
72. P. Ji, B. Shang, Q. Peng, X. Hu and J. Wei, *J. Power Sources*, **400**, 572 (2018).
73. S. H. Chung and A. Manthiram, *Adv. Mater.*, **30**, 1705951 (2018).
74. J. Wu, Z. Pan, Y. Dai, T. Wang, H. Zhang, S. Yan, J. Xu and K. Song, *J. Alloys Compd.*, **823**, 153912 (2020).
75. J. Wang, L. Lu, D. Shi, R. Tandiono, Z. Wang, K. Konstantinov and H. Liu, *ChemPlusChem*, **78**, 318 (2013).
76. X. Lang, Y. Zhao, K. Cai, L. Li, D. Chen and Q. Zhang, *Energy Technol.*, **7**, 1900543 (2019).
77. X. Chen, G. Du, M. Zhang, A. Kalam, S. Ding, Q. Su, B. Xu and A. G. Al-Sehemi, *Energy Technol.*, **8**, 1901163 (2019).
78. S. Peng, C. Wang, S. Yan, N. Wang, J. Wang and S. Dai, *ChemElectroChem*, **6**, 3291 (2019).
79. Y. Zhang, J. Ren, D. Wang, C. Zhang, F. Yin, A. Mukanova and Z. Bakenov, *ChemElectroChem*, **5**, 1591 (2018).
80. H. J. Peng, J. Q. Huang, X. B. Cheng and Q. Zhang, *Adv. Energy Mater.*, **5**, 1500408 (2015).
81. R. Yu, S.-H. Chung, C.-H. Chen and A. Manthiram, *Energy Storage Mater.*, **18**, 491 (2019).
82. R. Xu, J. Lu and K. Amine, *Adv. Energy Mater.*, **5**, 1500408 (2015).
83. S. H. Chung, C. H. Chang and A. Manthiram, *Adv. Funct. Mater.*, **28**, 1801188 (2018).
84. J. Song, T. Xu, M. L. Gordin, P. Zhu, D. Lv, Y. B. Jiang, Y. Chen, Y. Duan and D. Wang, *Adv. Funct. Mater.*, **24**, 1243 (2014).
85. R. Fang, G. Li, S. Zhao, L. Yin, K. Du, P. Hou, S. Wang, H.-M. Cheng, C. Liu and F. Li, *Nano Energy*, **42**, 205 (2017).
86. Z. Yuan, H.-J. Peng, T.-Z. Hou, J.-Q. Huang, C.-M. Chen, D.-W. Wang, X.-B. Cheng, F. Wei and Q. Zhang, *Nano Lett.*, **16**, 519 (2016).
87. M. Hagen, D. Hanselmann, K. Ahlbrecht, R. Maça, D. Gerber and J. Tübke, *Adv. Energy Mater.*, **5**, 1401986 (2015).
88. M. A. Pope and I. A. Aksay, *Adv. Energy Mater.*, **5**, 1500124 (2015).
89. D. Eroglu, K. R. Zavadil and K. G. Gallagher, *J. Electrochem. Soc.*, **162**, A982 (2015).
90. M.-Y. Chu, L. C. De Jonghe, S. J. Visco and B. D. Katz, *Google Patents*, 6,030,720 (2000).
91. Y. Fu, Y. S. Su and A. Manthiram, *Angew. Chem. Int. Ed.*, **52**, 6930 (2013).
92. X. Pu, G. Yang and C. Yu, *Adv. Mater.*, **26**, 7456 (2014).
93. X. Liu, Q. Zhang, J. Huang, S. Zhang, H. Peng and F. Wei, *J. Energy Chem.*, **22**, 341 (2013).
94. Y. Fu, Y. S. Su and A. Manthiram, *Angew. Chem.*, **125**, 7068 (2013).
95. Y. Zuo, Y. Zhu, X. Tang, M. Zhao, P. Ren, W. Su, Y. Tang and Y. Chen, *J. Power Sources*, **464**, 228181 (2020).
96. L. Jin, J. Ni, C. Shen, F. Peng, Q. Wu, D. Ye, J. Zheng, G. Li, C. Zhang, Z. Li and J. P. Zheng, *J. Power Sources*, **448**, 227336 (2020).
97. X. Liu, P. Chen, J. Chen, Q. Zeng, Z. Wang, Z. Li and L. Zhang, *Electrochim. Acta*, **330**, 135337 (2020).
98. W.-G. Lim, C. Jo, J. Lee and D. S. Hwang, *Korean J. Chem. Eng.*, **35**, 579 (2018).
99. Z. W. Seh, Y. Sun, Q. Zhang and Y. Cui, *Chem. Soc. Rev.*, **45**, 5605 (2016).
100. S.-H. Yeon, W. Ahn, K.-H. Shin, C.-S. Jin, K.-N. Jung, J.-D. Jeon, S. Lim and Y. Kim, *Korean J. Chem. Eng.*, **32**, 867 (2015).
101. H. Danuta and U. Juliusz, *Google Patents*, 3,043,896 (1962).
102. P. Cunningham, S. Johnson and E. Cairns, *J. Electrochem. Soc.*, **119**, 1448 (1972).
103. X. Ji, K. T. Lee and L. F. Nazar, *Nat. Mater.*, **8**, 500 (2009).
104. L. Ma, K. E. Hendrickson, S. Wei and L. A. Archer, *Nano Today*,

10, 315 (2015).
105. G.-L. Xu, Q. Wang, J.-C. Fang, Y.-F. Xu, J.-T. Li, L. Huang and S.-G. Sun, *J. Mater. Chem. A*, **2**, 19941 (2014).
106. S. H. Chung and A. Manthiram, *Adv. Funct. Mater.*, **24**, 5299 (2014).
107. J. Ming, M. Li, P. Kumar and L.-J. Li, *ACS Nano*, **10**, 6037 (2016).
108. B. Yan, X. Li, Z. Bai, X. Song, D. Xiong, M. Zhao, D. Li and S. Lu, *J. Power Sources*, **338**, 34 (2017).
109. X. Fang and H. Peng, *Small*, **11**, 1488 (2015).
110. D. Zheng, G. Wang, D. Liu, J. Si, T. Ding, D. Qu, X. Yang and D. Qu, *Adv. Mater. Technol.*, **3**, 1700233 (2018).
111. L. Zhou, D. L. Danilov, R. A. Eichel and P. H. Notten, *Adv. Energy Mater.*, **10**, 2001304 (2020).
112. R. Rauh, K. Abraham, G. Pearson, J. Surprenant and S. Brummer, *J. Electrochem. Soc.*, **126**, 523 (1979).
113. M. Vijayakumar, N. Govind, E. Walter, S. D. Burton, A. Shukla, A. Devaraj, J. Xiao, J. Liu, C. Wang and A. Karim, *Phys. Chem. Chem. Phys.*, **16**, 10923 (2014).
114. H. Lin, D.-D. Yang, N. Lou, A.-L. Wang, S.-G. Zhu and H.-Z. Li, *J. Appl. Phys.*, **125**, 094303 (2019).
115. D. Rao, L. Zhang, Y. Wang, Z. Meng, X. Qian, J. Liu, X. Shen, G. Qiao and R. Lu, *J. Phys. Chem. C*, **121**, 11047 (2017).
116. Y. Zhao and J. Zhao, *Appl. Surf. Sci.*, **412**, 591 (2017).
117. E. S. Sim, G. S. Yi, M. Je, Y. Lee and Y.-C. Chung, *J. Power Sources*, **342**, 64 (2017).
118. Q. Wang, J. Zheng, E. Walter, H. Pan, D. Lv, P. Zuo, H. Chen, Z. D. Deng, B. Y. Liaw and X. Yu, *J. Electrochem. Soc.*, **162**, A474 (2015).
119. X. Yu and A. Manthiram, *Phys. Chem. Chem. Phys.*, **17**, 2127 (2015).
120. M. U. Patel, R. Demir-Cakan, M. Morcrette, J. M. Tarascon, M. Gaberscek and R. Dominko, *ChemSusChem*, **6** , 1177 (2013).
121. S.-H. Chung, C.-H. Chang and A. Manthiram, *ACS Nano*, **10**, 10462 (2016).
122. G. Zhou, Y. Zhao, C. Zu and A. Manthiram, *Nano Energy*, **12**, 240 (2015).
123. G. Zhou, E. Paek, G. S. Hwang and A. Manthiram, *Nat. Commun.*, **6**, 1 (2015).
124. P. Chiochan, S. Kosasang, N. Ma, S. Duangdangchote, P. Suktha and M. Sawangphruk, *Carbon*, **158**, 244 (2020).
125. S. Li, J. Warzywoda, S. Wang, G. Ren and Z. Fan, *Carbon*, **124**, 212 (2017).
126. S. Niu, S.-W. Zhang, R. Shi, J. Wang, W. Wang, X. Chen, Z. Zhang, J. Miao, A. Amini, Y. Zhao and C. Cheng, *Energy Storage Mater.*, **33**, 73 (2020).
127. S.-H. Chung, L. Luo and A. Manthiram, *ACS Energy Lett.*, **3**, 568 (2018).
128. G. Zhou, Y. Zhao, C. Zu and A. Manthiram, *Nano Energy*, **12**, 240 (2015).
129. S. Chen, Y. Gao, Z. Yu, M. L. Gordin, J. Song and D. Wang, *Nano Energy*, **31**, 418 (2017).
130. M. Barghamadi, A. S. Best, A. I. Bhatt, A. F. Hollenkamp, M. Musameh, R. J. Rees and T. Rüther, *Energy Environ. Sci.*, **7**, 3902 (2014).
131. C. Zu, Y. Fu and A. Manthiram, *J. Mater. Chem. A*, **1**, 10362 (2013).
132. S. D. Talian, J. Bobnar, J. Moškon, R. Dominko and M. Gaberšček, *Electrochim. Acta*, **354**, 136696 (2020).
133. S. Kim, H. Song and Y. Jeong, *Carbon*, **113**, 371 (2017).
134. S. Liatard, K. Benhamouda, A. Fournier, R. Ramos, C. Barchasz and J. Dijon, *ChemComm*, **51**, 7749 (2015).
135. S. Liatard, K. Benhamouda, A. Fournier, J. Dijon and C. Barchasz, *Electrochim. Acta*, **187**, 670 (2016).
136. C. Qu, Y. Chen, X. Yang, H. Zhang, X. Li and H. Zhang, *Nano Energy*, **39**, 262 (2017).
137. J. Li, N. Lotfi, R. G. Landers and J. Park, *J. Electrochem. Soc.*, **164**, A874 (2017).
138. V. Thangavel, K.-H. Xue, Y. Mammeri, M. Quiroga, A. Mastouri, C. Guéry, P. Johansson, M. Morcrette and A. A. Franco, *J. Electrochem. Soc.*, **163**, A2817 (2016).
139. D. Eroglu, K. R. Zavadil and K. G. Gallagher, *J. Electrochem. Soc.*, **162**, A982 (2015).
140. Y. V. Mikhaylik and J. R. Akridge, *J. Electrochem. Soc.*, **151**, A1969 (2004).
141. B. D. McCloskey, *J. Phys. Chem. Lett.*, **6**, 4581 (2015).
142. Y. Li, S. Yao, C. Zhang, Y. He, Y. Wang, Y. Liang, X. Shen, T. Li, S. Qin and W. Wen, *Int. J. Energy Res.*, **44**, 8388 (2020).
143. L. Qie, C. Zu and A. Manthiram, *Adv. Energy Mater.*, **6**, 1502459 (2016).
144. R. Fang, S. Zhao, Z. Sun, D. W. Wang, H. M. Cheng and F. Li, *Adv. Mater.*, **29**, 1606823 (2017).
145. J. Scheers, S. Fantini and P. Johansson, *J. Power Sources*, **255**, 204 (2014).
146. J. Zheng, D. Lv, M. Gu, C. Wang, J.-G. Zhang, J. Liu and J. Xiao, *J. Electrochem. Soc.*, **160**, A2288 (2013).
147. S.-H. Chung and A. Manthiram, *ACS Appl. Mater. Interfaces*, **10**, 43749 (2018).
148. M. Jana, R. Xu, X.-B. Cheng, J. S. Yeon, J. M. Park, J.-Q. Huang, Q. Zhang and H.S. Park, *Energy Environ. Sci.*, **13**, 1049 (2020).
149. R. Yu, S.-H. Chung, C.-H. Chen and A. Manthiram, *J. Mater. Chem. A*, **6**, 24841 (2018).
150. Y. Chen, S. Liu, X. Yuan, X. Hu, W. Ye, A. A. Razzaq, Y. Lian, M. Chen, X. Zhao, Y. Peng, J.-H. Choi, J.-H. Ahn and Z. Deng, *Carbon*, **167**, 446 (2020).
151. S. Liatard, K. Benhamouda, A. Fournier, J. Dijon and C. Barchasz, *Electrochim. Acta*, **187**, 670 (2016).

Jung Sang Cho received his Ph. D. from interdisciplinary program for bioengineering, college of engineering, Seoul national university, Korea in 2013, and had post-doc experience at the department of materials science and engineering, Korea university, Korea (2014-2016). He is currently a professor at the department of engineering chemistry, chungbuk national university, Korea since 2016. His research group works on the development of nanostructured materials for the energy storage, sensor, catalyst, display, and biomaterials. For details, please see the lab website: https://jjj777.wixsite.com/professor-cho/members.